JOURNAL OF APPLIED PHYSICS VOLUME 84, NUMBER 11 1 DECEMBER 1998

Growth of poly- and single-crystal ScN on MgO(001): Role of low-energy N_2^+ irradiation in determining texture, microstructure evolution, and mechanical properties

D. Gall and I. Petrov
Department of Materials Science, Coordinated Science Laboratory, and Materials Research Laboratory, University of Illinois, 1101 West Springfield Avenue, Urbana, Illinois 61801

N. Hellgren, L. Hultman, and J. E. Sundgren
Department of Physics, Thin Films Division, Linköping University, S-581 83 Linköping, Sweden

J. E. Greene[a)]
Department of Materials Science, Coordinated Science Laboratory, and Materials Research Laboratory, University of Illinois, 1101 West Springfield Avenue, Urbana, Illinois 61801

(Received 2 June 1998; accepted for publication 27 August 1998)

ScN layers, 345 nm thick, were grown on MgO(001) substrates at 750 °C by ultrahigh-vacuum reactive magnetron sputter deposition in pure N_2 discharges at 5 mTorr. The N_2^+ to Sc ratio incident at the substrate and growing film was maintained constant at 14, while the ion energy $E_{N_2^+}$ was varied from 13 to 50 eV. All films were stoichiometric with N/Sc ratios of 1.00 ± 0.02. However, microstructural and surface morphological evolution were found to depend strongly on $E_{N_2^+}$. The nucleation and initial growth stages of ScN films deposited with $E_{N_2^+} = 13$ eV are dominated by the formation of 111- and 002-oriented islands, but preferred orientation rapidly evolves toward a purely 111 texture by a film thickness of $\simeq 50$ nm as 002 grains grow out of existence in a kinetically limited competitive growth mode. In distinct contrast, films deposited with $E_{N_2^+} = 20$ eV grow in a cube-on-cube epitaxial relationship with the substrate and exhibit no indication of 111-oriented grains, even in the earliest stages. Increasing $E_{N_2^+}$ to 50 eV still results in epitaxial layers, but with high in-plane compressive stress and the presence of N_2 gas bubbles. All epitaxial layers contain rectangular nanopipes $\simeq 1$ nm wide and aligned along the growth direction. The nanopipes result from atomic shadowing near the bottom of a periodic array of surface cusps which form along orthogonal $\langle 100 \rangle$ directions due to kinetic roughening during growth. The hardness H and elastic modulus E of the epitaxial ScN(001) layer grown with $E_{N_2^+} = 20$ eV are 21.1 ± 1.1 and 356 ± 18 GPa, respectively. H and E increase (decrease) with increasing (decreasing) $E_{N_2^+}$.
© *1998 American Institute of Physics.* [S0021-8979(98)01623-5]

I. INTRODUCTION

Transition-metal nitrides are well known for their remarkable physical properties including high hardness and mechanical strength, chemical inertness, and electrical resistivities that vary from metallic to semiconducting. As a result, they are widely studied and have become technologically important for applications such as hard wear-resistant coatings, diffusion barriers, and optical coatings. While TiN has received by far the most attention and is presently used commercially in all of the above mentioned applications, the neighboring nitride on the periodic table, ScN, is almost totally unexplored.[1]

Published theoretical data on the electronic structure of ScN are contradictory. Self-consistent augmented plane-wave band structure calculations by Neckel *et al.*[2] predict a very small, 0.01 eV, overlap of N 2p valence and Sc 3d conduction bands, leading to metallic conductivity. However, the uncertainty in the relative energy positions of the bands in these calculations is 1 eV and the results are therefore not sufficiently accurate to conclude whether or not there is band overlap in the ScN density of states.[3] Johansson *et al.*[4] compared electronic structure calculations for TiN with angle-resolved photoelectron spectroscopy data and found significant differences at high symmetry points in the Brillouin zone. The energy of the Δ_5 valence band at the Γ point was predicted 1 eV too high and the $\Delta_{2'}$ conduction band at the X point was 1 eV too low. In the bandstructure calculations for ScN, these two points define the overlap of valence and conduction band which means that, assuming a similar error in the ScN calculations, ScN could have a band gap of $\geqslant 2$ eV.

We have recently shown, based upon temperature-dependent resistivity, optical absorption and reflectivity, and spectroscopic ellipsometry measurements carried out on polycrystalline ScN films deposited on MgO(001)[1] and epi-

[a)]Also at Department of Physics, Thin Films Division, Linköping University, S-581 83 Linköping, Sweden; electronic mail: jegreene@uiuc.edu

 © 1998 American Institute of Physics

taxial ScN layers grown on TiN/MgO(001)[5] by ultrahigh vacuum (UHV) reactive magnetron sputter deposition, that ScN is a semiconductor. The direct optical band gap was determined to be 2.37 and 2.32 eV for polycrystalline and single-crystal ScN, respectively.

In this article, we present the results of an investigation of the effects of low-energy N_2^+ ion irradiation on microstructural and texture evolution, as well as the mechanical properties, of polycrystalline and epitaxial ScN layers grown on MgO(001) by UHV reactive magnetron sputtering in pure N_2 discharges. The films, 345 nm thick, were deposited with a very high incident ion N_2^+ to Sc ratio, $J_{N_2^+}/J_{Sc}=14$, shown previously to have a major effect on the texture of polycrystalline TiN (Ref. 6) and $Ti_{1-x}Al_xN$ (Ref. 7) films, while the ion energy $E_{N_2^+}$ was varied from 13 to 50 eV. All films were stoichiometric with N/Sc ratios of 1.00 ± 0.02. Nucleation and initial growth of ScN films deposited with $E_{N_2^+}=13$ eV are dominated by the formation of 111- and 002-oriented islands. However, preferred orientation rapidly evolves toward a purely 111 texture within a thickness of $\simeq 50$ nm as the 002 grains grow out of existence. Films deposited with $E_{N_2^+}=20$ eV are epitaxial and grow with a cube-on-cube relationship with the substrate while ScN(001) layers grown with $E_{N_2^+}=50$ eV, although still epitaxial, exhibit high in-plane compressive stress with elongated gas bubbles containing excess nitrogen. All epitaxial layers contain nanopipes, with rectangular cross sections $\simeq 1$ nm wide and aligned along the growth direction, associated with surface cusps which form due to kinetic roughening during film growth.[8]

Epitaxial ScN(001) layers grown with $E_{N_2^+}=20$ eV have hardness and elastic modulus values of 21 and 356 GPa compared with 20 and 445 GPa for TiN(001) reference samples. Measured film hardness and elastic moduli increase with increasing $E_{N_2^+}$ due to ion-irradiation-induced in-plane compressive strain.

II. EXPERIMENTAL PROCEDURE

All films were grown in a two-chamber turbomolecular-pumped UHV deposition system. The apparatus consists of a sample introduction chamber, evacuated to 5×10^{-8} Torr (6.7×10^{-6} Pa) prior to sample transfer, and a three-target magnetron growth chamber with a base pressure of 1×10^{-9} Torr (1.3×10^{-7} Pa). The target was a 5-cm-diam water-cooled Sc disk, 99.9% pure with the only detectable contaminant being 0.1 at % Ta, the usual impurity in Sc. Sputtering was carried out in pure N_2 (99.999%), introduced through a high precision solenoid valve, at 5 mTorr (0.7 Pa). The pressure was measured by a capacitance manometer and maintained constant with an automatic mass-flow controller. A power-regulated dc supply was used to provide a discharge current of 1.7 A and a target voltage of 300 V which, with a target-to-substrate separation of 15 cm, resulted in a film deposition rate of 173 nm h^{-1} in the fully target-nitrided regime. The target was sputter etched for 5 min, with a shutter shielding the substrate, prior to initiating deposition.

The substrates were polished $10\times10\times0.5$ mm^3 MgO(001) wafers which were cleaned and degreased by successive rinses in ultrasonic baths of trichloroethane, acetone, methanol, and deionized water and then blown dry in dry N_2. They were mounted on resistively-heated Ta platens using Mo clips and inserted into the sample introduction chamber for transport into the deposition chamber. Final substrate cleaning consisted of thermal degassing at 800 °C for 1 h, a procedure shown to result in sharp MgO(001)1×1 reflection high energy electron diffraction patterns.[9] Film growth temperature, 750 °C including the contribution due to plasma heating, was measured using a pyrometer calibrated by a thermocouple bonded to a dummy MgO wafer. Following deposition, the samples were allowed to cool to <100 °C before transferring them to the load-lock chamber which was then vented with dry N_2.

A 25-cm-diam coil was used to magnetically unbalance the discharge.[10] The coil, maintained at floating potential with a constant current of 3 A, provided a maximum field between the target and substrate of 80 G which was additive to that of the permanent magnets behind the target. This has the effect of focusing the discharge to greatly increase the plasma density near the substrate while having only a minor effect on the target sputtering rate.[10] The applied substrate bias V_s during film growth was varied between 0 and -50 V.

Plasma characteristics in the vicinity of the substrate during film growth were determined from probe measurements following the procedures described in Ref. 10. The current-measuring probe was a 6-mm-diam ScN-coated stainless-steel disk mounted in a through-hole drilled in the center of a special substrate platten. The probe was situated such that its surface was in the plane of the substrate and it was electrically isolated from the platten by a 0.25 mm vacuum gap. To minimize edge effects, the probe and substrate holder were maintained at the same potential with respect to the anode.

The vast majority of the ions incident at the substrate and growing film during deposition experienced the full sheath potential since the mean-free path for charge-exchange collisions, $\simeq 8$ mm,[11] was more than an order of magnitude larger than the sheath width, estimated from the Child–Langmuir equation[12] and the measured current density, $j_i=0.48$ mA cm^{-2}, to range from 0.3 mm at $V_s=13$ V to 0.8 mm at $V_s=50$ V. N_2^+ ions accelerated to energies greater than their molecular binding energy of 9.7 eV (Ref. 13) dissociate upon collision with the film surface.

Film microstructure and texture were investigated using a combination of x-ray diffraction (XRD), plan-view transmission electron microscopy (TEM), and cross-sectional TEM (XTEM). The XRD measurements were carried out in a powder diffractometer system with a Cu $K\alpha$ source and slit divergences of 1° and 0.1° for θ–2θ scans and ω-rocking curves, respectively. The resulting resolution was 0.01° 2θ and 0.1° ω. TEM and XTEM analyses were performed in a Phillips CM12 microscope with a LaB_6 filament at 120 kV. Plan-view specimens were prepared by mechanically thinning from the backside with SiC to a specimen thickness of $\simeq 30$ μm. Final thinning to electron transparency was accomplished by ion milling using a 5.5 kV Ar^+ ion beam incident initially at 14° and then decreased to 12°. Cross-

sectional specimens were prepared by gluing two samples film-to-film and then cutting vertical sections which were ground and milled in a manner similar to that of the plan-view samples, but from both sides.

The microchemistry of as-deposited films was examined by Rutherford backscattering spectroscopy (RBS). The probe beam consisted of 2 MeV He^+ ions incident at an angle of 22.5° relative to the sample surface normal with the detector set at a 150° scattering angle. Backscattered spectra were analyzed to determine N/Sc ratios using the RUMP simulation program.[14]

Nanoindentation responses of as-deposited ScN films were determined using a Nano Indentor II instrument. Epitaxial TiN layers, also grown on MgO(001) and having the same thickness as the ScN samples, served as references for calibration purposes.[15] The measurement procedure was as follows:[15] load to maximum, unload to 10% of maximum load, hold for 50 s, load to maximum, hold for 200 s, and completely unload. The maximum load was varied from 0.4 to 40 mN and a minimum of ten indent sequences was used for each maximum load. The triangular Berkovich diamond tip was calibrated following the procedure described in Ref. 16.

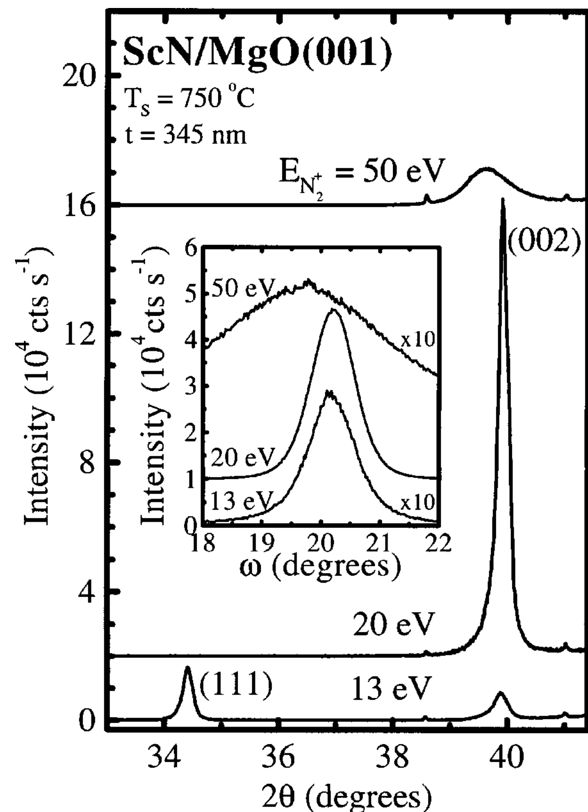

FIG. 1. XRD θ–2θ scans from 345-nm-thick ScN films grown at 750 °C on MgO(001) by UHV reactive magnetron sputter deposition with an incident N_2^+ to Sc flux ratio of 14 and $E_{N_2^+}=13$, 20, and 50 eV. The inset shows corresponding ScN(002) ω-rocking curves.

III. RESULTS AND DISCUSSION

The plasma characterization experiments showed that the substrate floating potential V_f during deposition was -13 V, while the plasma potential V_p was estimated from the measured electron temperature, 2.6 ± 0.2 eV, to be 0 ± 1 V. The plasma ion density near the substrate and the saturation ion current density to the substrate were 1.7×10^{10} cm^{-3} and 0.48 mA cm^{-2}, respectively, corresponding to an ion flux of 3×10^{15} cm^{-2} s^{-1}. This yields, when combined with the measured film deposition rate, a N_2^+-to-Sc ratio $J_{N_2^+}/J_{Sc}=14$. Based upon energy- and mass-resolved analyses of ions incident at the substrate during reactive magnetron sputtering of Ti in pure N_2 discharges,[17] the dominant (>96%) ion species is N_2^+. In this article, we focus on the growth of ScN films deposited with very high ion-to-metal ratios, shown previously to have a major effect on the texture of polycrystalline TiN[6] and $Ti_{1-x}Al_xN$[7] films, and ion energies $E_{N_2^+}=13$, 20, and 50 eV.

All ScN layers, independent of $E_{N_2^+}$, were found from RBS analyses to be stoichiometric with N/Sc ratios of 1.00 ± 0.02.

A. Microstructural and surface morphological evolution

Typical XRD θ–2θ scans, offset for clarity of presentation, are presented in Fig. 1. Scans from films grown with $E_{N_2^+}=13$ eV show that the layers are polycrystalline and exhibit 111 and 002 ScN diffraction peaks. The ratio of the 111 to 002 integrated peak intensities I_{111}/I_{002} is 1.94 compared with an expected ratio of 0.66 (Ref. 18) for randomly oriented ScN powder samples. The $E_{N_2^+}=13$ eV films thus have a dominant 111 texture. The small peaks at 38.60 and 41.04° 2θ (present in all scans) are MgO 002 substrate reflections originating from Cu $K\beta$ and W$L\alpha_1$ contamination in the x-ray source.

XRD scans from films grown with $E_{N_2^+}=20$ and 50 eV contain only 002 ScN diffraction peaks. However, while the 002 peak is relatively intense, with $I=1.4\times10^5$ cts s^{-1}, and sharp (full width at half maximum intensity $\Gamma_{2\theta}=0.21°$ 2θ) in the $E_{N_2^+}=20$ eV scan, the $E_{N_2^+}=50$ eV 002 peak is weaker ($I=1.1\times10^4$ cts s^{-1}), broader ($\Gamma_{2\theta}=0.92°$ 2θ), and shifted by 0.28° to a lower 2θ position. These results indicate that, compared to the $E_{N_2^+}=20$ eV epitaxial layer, the 50 eV film has a high defect density and is expanded along the growth direction. The latter is the signature of significant residual in-plane compressive strain.

The 111 and 002 peak positions obtained from the 13 eV film yield lattice constants in the growth direction of 0.4509 and 0.4516 nm, respectively, slightly higher than the relaxed ScN lattice constant $a_0=0.4501$ nm.[5] This corresponds to an in-plane compressive stress of $\simeq2$ GPa (Ref. 19) which can be completely explained by differential thermal contraction during cooling from the deposition temperature, 750 °C. The thermal expansion coefficients of ScN and MgO are 4×10^{-6} (Ref. 20) and 1.3×10^{-5} K^{-1} (Ref. 21), respectively. The measured difference in 111 and 002 lattice constants is partially due to residual misfit-induced strain in 002 grains, which exhibit local epitaxy, giving rise to a larger local strain. In addition, we expect that, as is the case for

other NaCl-structure transition-metal nitrides such as TiN,[22] the elastic modulus of ScN is directionally anisotropic.

Based upon the measured θ–2θ peak intensity ratio I_{111}/I_{002} normalized to the randomly oriented value and accounting for the large difference in azimuthal 111 vs 002 grain alignment as determined from the ω-rocking curves, we estimate that the ratio of the 111 to 002 volume fractions in 13 eV films is 11 ± 3.

ScN(002) films grown with $E_{N_2^+}=20$ eV are also slightly in compression due to film/substrate differential thermal contraction and exhibit a measured perpendicular lattice constant of 0.4512 nm. However, the 50 eV layers have a perpendicular lattice constant of 0.4542 nm, 0.9% larger than the relaxed value and much too large to be completely explained by differential thermal contraction. The relatively large in-plane compressive stress, $\simeq 12$ GPa, is most likely due to a combination of residual ion-irradiation-induced defects and implanted interstitial N. The average kinetic energy per N atom upon dissociative collision of 50 eV N_2^+ ions at the growing film surface is above the expected lattice displacement energy for ScN.

The inset in Fig. 1 shows corresponding 002 ω-rocking curves from the same three films used to obtain the θ–2θ scans. The intensities of the 13 and 50 eV rocking curves are multiplied by a factor 10 and all scans are offset vertically. The full widths at half maximum intensities Γ_ω of 002 rocking curves from layers grown with $E_{N_2^+}=13$, 20, and 50 eV are 0.950, 0.870, and 3.12°. Γ_ω for the 111 ScN peak from the 13 eV layer (not shown) is 2.13°.

In-plane and perpendicular (along the film growth direction) x-ray coherence lengths $\xi_\parallel$ and $\xi_\perp$ can be obtained from the widths of the diffracted intensity distributions perpendicular $\Delta g_\perp$ and parallel $\Delta g_\parallel$, respectively, to the diffraction vector $\bar{g}$ using the relationships[9]

$$\xi_\parallel=\frac{2\pi}{|\Delta g_\perp|}=\frac{\lambda}{2\Gamma_\omega \sin\theta} \tag{1}$$

and

$$\xi_\perp=\frac{2\pi}{|\Delta g_\perp|}=\frac{\lambda}{\Gamma_{2\theta}\cos\theta}, \tag{2}$$

where λ is the x-ray wavelength. From the data presented in Fig. 1, $\xi_\parallel$ and $\xi_\perp$ are 15 and 57 nm for the ScN film grown with $E_{N_2^+}=20$ eV and 4 and 10 nm for the 50 eV layer. Thus, the mosaic domain size is approximately a factor of 5 smaller, in both directions, in the 50 eV films due to residual ion-irradiation-induced damage.

Figure 2 is an XTEM micrograph from a ScN film deposited with $E_{N_2^+}=13$ eV. The layer has a columnar structure which, based upon lower magnification XTEM micrographs together with plan-view TEM images, has an average column width of 30 nm. The corresponding selected area electron diffraction (SAED) pattern (left inset in Fig. 2) was obtained using a 0.4-μm-diam aperture centered at the ScN/MgO interface. It is composed of 002 and 111 diffraction spots corresponding to MgO 002 and ScN 111 interplanar spacings $d_\perp$ of 0.21 and 0.26 nm, respectively, along the growth direction. This is in very good agreement with the ScN XRD results for which $d_{\perp,111}=0.2603$ nm.

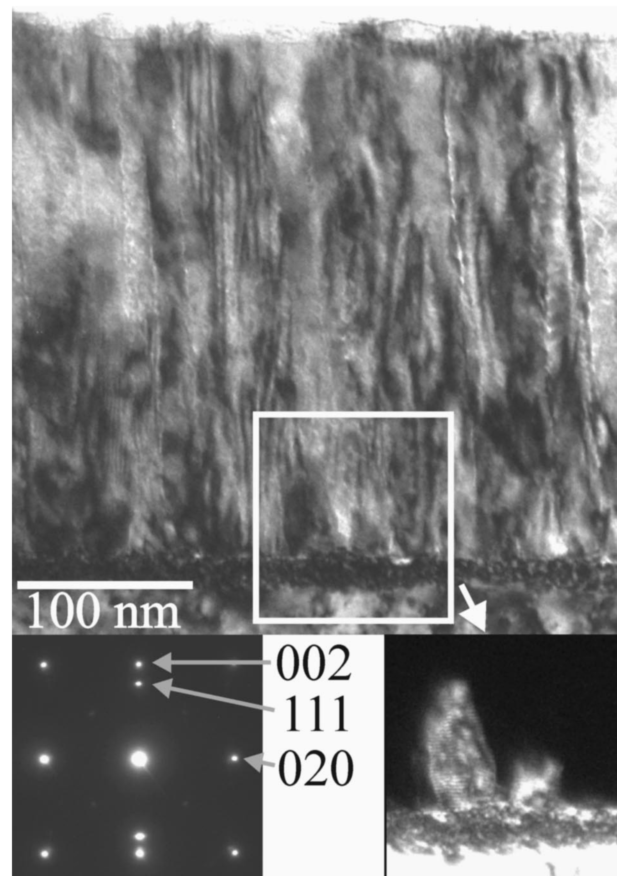

FIG. 2. (a) Bright-field [100] XTEM micrograph of a 345-nm-thick ScN film grown at 750 °C on MgO(001) by UHV reactive magnetron sputter deposition with $J_{N_2^+}/J_{Sc}=14$ and $E_{N_2^+}=13$ eV. The lower left inset is a corresponding SAED pattern and the right inset is a dark-field micrograph obtained using the 020 reflection.

The discrete nature of the ScN electron diffraction features reflects the strong 111 film texture. Diffraction spots from 002-oriented ScN grains cannot be resolved from the stronger MgO reflections indicating, again in agreement with XRD results, that the film contains only a small volume fraction of 002 grains. This is confirmed in the dark-field XTEM micrograph (right inset, Fig. 2), obtained using the diffraction spot labeled 020 in the SAED pattern (left inset, Fig. 2), from the region outlined in the bright-field image. Under these imaging conditions, MgO and 002-oriented ScN grains appear bright, while 111-oriented ScN remains dark. Consistent with the dark-field image in Fig. 2, extensive analyses establish that all ScN 002 grains are located at the bottom of the film and terminate at distances of 5–50 nm from the substrate surface as they are overgrown by 111-oriented columns. These results are similar to those reported earlier for ScN layers grown without enhanced N_2^+ irradiation.[1]

Due to the structural and bonding similarities between ScN and TiN, we assume that, as is the case for TiN,[23] the lowest surface energy face of ScN is (001). Hence, (001) is expected to be the preferred orientation under growth conditions where adatom mobilities are sufficiently high to favor crystallites bounded by low-energy planes. Strain can also

provide a driving force for the development of preferred orientation in materials such as transition-metal (TM) nitrides which typically have highly anisotropic elastic moduli. However, we showed earlier that ScN layers deposited with $E_{N_2^+}=13$ eV had no significant strain during growth. Thus, the eventual dominance of the 111 vs 002 ScN texture that we observe during competitive columnar growth must be due to kinetic limitations during film growth rather than thermodynamic driving forces.

Similar results in which the higher-energy surface emerges as the preferred orientation have been reported for TiN,[6] $Ti_{0.5}Al_{0.5}N$,[7] and Monte Carlo simulations of fcc film growth.[24] In each of these cases, the effect can be explained as being due to anisotropies in surface diffusivities. That is, during growth under relatively low adatom mobility conditions, the average adatom residence time is significantly higher at sites on low diffusivity vs high diffusivity surfaces. Thus, adatoms which are deposited near grain boundaries and sample sites on both sides of the boundary have a higher probability of finally being incorporated into the low-diffusivity grain. Conversely, adatoms on high diffusivity planes have larger mean-free paths with correspondingly higher probabilities to move off the plane and become trapped on adjacent grains. Thus, at low homologous deposition temperatures T_s/T_m (T_m is the melting point expressed in K), grains with low surface diffusivities can grow at the expense of their neighbors.[25]

For the growth of TM nitrides by reactive sputter deposition, the rate limiting step is cation incorporation since the nitrogen supply rate is typically orders of magnitude larger and dissociative chemisorption of N_2 at available TM sites occurs at near kinetic rates. In the particular case of NaCl-structure TM nitrides such as ScN (and TiN), we expect cation mobilities to be lower on (111) surfaces to which they have three backbonds than on (002) with which they have one backbond. Therefore, we propose that the above described mechanism associated with anisotropic cation surface diffusivity controls the development of 111 preferred orientation in films deposited with $E_{N_2^+}=13$ eV.

Figure 3(a) is an XTEM image of a ScN layer deposited with 20 eV N_2^+ irradiation. The film is epitaxial with no indication, either in cross-sectional or plan-view micrographs, of the presence of grain boundaries. The corresponding SAED pattern, shown as an inset, consists of overlapping symmetric 002 and 022 reflections signifying a cube-on-cube epitaxial relationship, $(001)_{ScN}\|(001)_{MgO}$ with $[100]_{ScN}\|[100]_{MgO}$, between MgO and ScN. In agreement with the XRD results, the film is nearly fully relaxed (bulk film/substrate lattice constant mismatch=7%).

The micrograph in Fig. 3(a) was acquired with the microscope deliberately underfocused such that underdense regions appear brighter. Careful observation reveals the presence of nanopipes along the film [001] growth direction. The majority of the nanopipes start at a film thickness t of approximately 5 nm and extend to the film surface. Figure 3(b), one of a series of images obtained following step-wise ion milling through the film from both sides, is a plan-view micrograph from the center of the 345-nm-thick $E_{N_2^+}=20$ eV

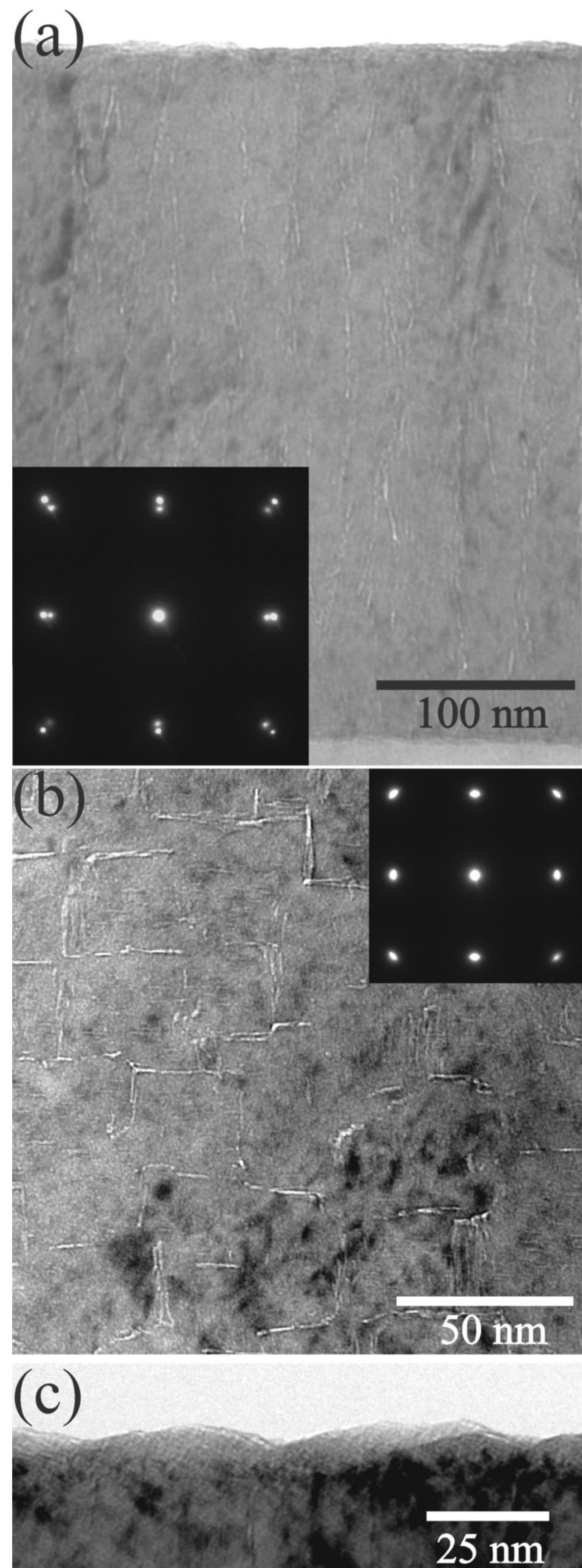

FIG. 3. (a) Bright-field [100] XTEM and (b) plan-view TEM images of a 345-nm-thick ScN film grown at 750 °C on MgO(001) by UHV reactive magnetron sputter deposition with $J_{N_2^+}/J_{Sc}=14$ and $E_{N_2^+}=20$ eV. The insets in (a) and (b) are corresponding SAED patterns. (c) Higher-resolution XTEM micrograph showing the near-surface region of the same sample.

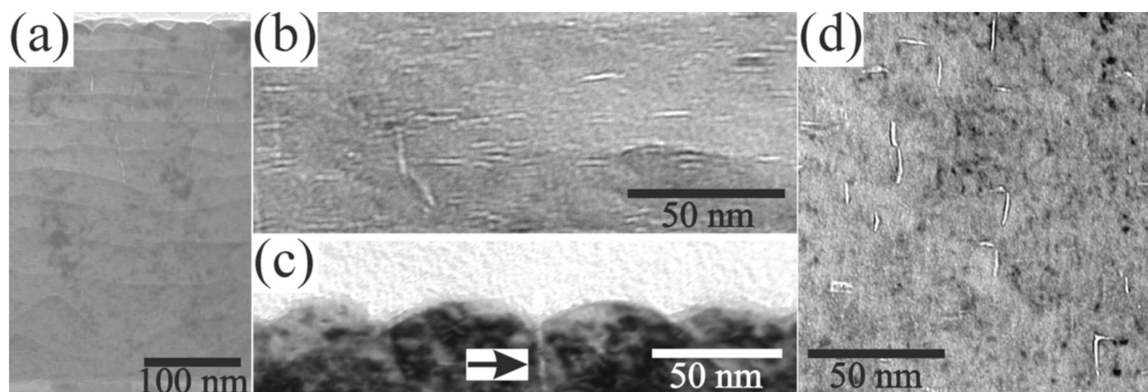

FIG. 4. (a) and (b): bright-field [100] XTEM micrographs, obtained at different magnifications, of a 345-nm-thick ScN film grown at 750 °C on MgO(001) by UHV reactive magnetron sputter deposition with $J_{N_2^+}/J_{Sc}=14$ and $E_{N_2^+}=50$ eV. (c) XTEM image showing the near-surface region of the same sample. (d) Plan-view TEM image.

layer corresponding to Fig. 3(a). The nanopipes are rectangular in cross section with a width of $\simeq 1$ nm by 1–15 nm along orthogonal ⟨100⟩ directions.

The surfaces of $E_{N_2^+}=20$ eV samples are rough [see, for example, the XTEM micrograph in Fig. 3(c)] and consist of mound structures characteristic of kinetic roughening as observed previously in both semiconductor,[8,26–29] metal,[30] and TM nitride[31,32] films grown at relatively low homologous temperatures. The primary origin of kinetic roughening is the presence of Ehrlich barriers,[33] and/or deep traps at step edges,[34] to the migration of adatoms over down-steps on growing surfaces. This leads to a divergence in adatom flux and, hence, increased nucleation on terraces which, in turn, gives rise to surface roughening and, eventually, facetting with increasing film thickness. XTEM images reveal that the surface morphology is periodic with an average surface width (root-mean-square mound height) of $\simeq 4$ nm and a lateral center-to-center mound correlation length (obtained from plan-view TEM images) of 30 ± 5 nm. The mounds adjoin along ⟨100⟩ directions with the development of deep cusps. The deposition rate at the bottom of a cusp is reduced due to atomic shadowing and leads, in combination with limited adatom mobility, to the formation of the nanopipes. The number density of nanopipes, $\simeq 3\times 10^3\ \mu\text{m}^{-2}$, correlates with the average mound spacing.

Figures 4(a) and 4(b) are XTEM micrographs, obtained at different magnifications, of a ScN layer deposited with $E_{N_2^+}=50$ eV. This film, like the 20 eV layer, is epitaxial and cross-sectional SAED patterns (not shown) are similar to the one in Fig. 3. Underfocused micrographs reveal that the 50 eV layer also contains vertical nanopipes, but with a lower number density ($\simeq 3\times 10^2\ \mu\text{m}^{-2}$). However, Fig. 4(b) shows that the film has a high density ($\simeq 2\times 10^5\ \mu\text{m}^{-3}$) of elongated horizontal defects (not present in the 20 eV layers) with average size 7×1.5 nm. These defects are formed during film growth by the agglomeration of trapped excess nitrogen similar to what has been observed in epitaxial TiN layers grown at 550 °C with higher $E_{N_2^+}$, 400 eV, but with a much lower ion to metal ratio, 1.3.[35] We estimate the amount of excess nitrogen in the observed defects to be $\leqslant 1$ at %, too small to be detected by RBS.

Combined XTEM and TEM analyses reveal that $E_{N_2^+}=50$ eV samples also exhibit a periodic surface morphology [see Fig. 4(c)], but with both a larger surface width, $\simeq 10$ nm, and a larger lateral correlation length, 50 ± 10 nm, than obtained with $E_{N_2^+}=20$ eV films. The latter is consistent with the smaller nanopipe number density in $E_{N_2^+}=50$ eV samples [see Fig. 4(d)] as well as the larger cross-sectional area, 1 nm width by up to 25 nm in the orthogonal in-plane direction. Figure 4(c) shows a nanopipe, labeled with an arrow, extending from the bottom of a surface cusp. We ascribe the larger surface roughness observed in 50 eV, compared to 20 eV, films to the higher residual ion-irradiation-induced defect density. Similar results were reported for epitaxial TiN layers deposited by reactive magnetron sputtering and examined by *in situ* scanning tunneling microscopy.[32]

B. Mechanical properties

The hardness and elastic moduli of our ScN layers were determined from nanoindentation measurements following the technique developed in Ref. 15 for epitaxial 001, 011, and 111 TiN. In fact, TiN(001) layers, grown on MgO under the same conditions as in Ref. 15, were measured before and after each ScN film and used for both calibration and reference purposes. The nanoindentation measurements were carried out using a three-sided pyramidal Berkovich diamond indentor tip operated at loads ranging from 0.4 to 40 mN.

Figure 5 shows a typical load-displacement curve, with a 4 mN maximum load, obtained from a ScN(001) layer grown at 750 °C with $E_{N_2^+}=20$ eV and $J_{N_2^+}/J_{Sc}=14$. A double loading cycle with a 50 s hold period after the first unloading sequence and a second hold segment of 200 s at maximum load was used in order to minimize the effects of time-dependent plasticity on the measured hardness. The initial loading segment contains an elastic-plastic displacement. The first unloading curve and the second loading curve differ substantially and form a hysteresis loop with a larger displacement during unloading than loading. The data from the first hold segment (50 s) were used to automatically correct the load-displacement data for thermal drift through the in-

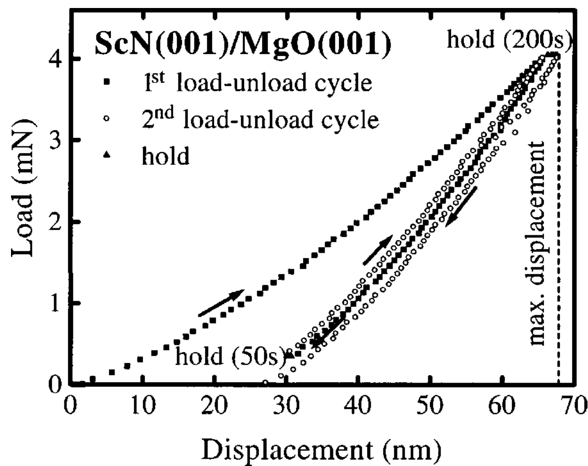

FIG. 5. Typical load-displacement curves (maximum load=4 mN) obtained during nanoindentation measurements of a ScN(001) film grown with $J_{N_2^+}/J_{Sc}=14$ and $E_{N_2^+}=20$ eV. Hold segments are labeled and the arrows indicate the load/unload directions.

strument software while the second hold was used to investigate creeplike plastic behavior. Approximately 2 nm of creep (dislocation nucleation, glide, and thermal drift) occurred at the maximum-load hold segment in Fig. 5. The percentage of elastic recovery was $\simeq 60\%$. A larger amount of thermal drift was observed at the longer second hold due, in addition to larger sensitivity to temperature fluctuations, to heating of the indenter by the loading coil. Indentation experiments in a fused-silica reference sample were used to determine the upper limit on thermal drift to be 5 nm at 4 mN maximum load for 200 s.

Measured hardness H values for all films, TiN reference samples and ScN, were found to exhibit a continuous decrease with increasing maximum displacement h_{max} due to two competing effects.[15] At very low displacements, the measured hardness is higher than bulk values due to a residual gradient in the near-surface defect concentration which, for TiN, can be removed by rapid thermal annealing for 30 s at 1000 °C.[15] In contrast, at high loads, the plastic zone associated with the indentation measurement penetrates through a significant fraction of the film thickness. This results in an apparent decrease in H for hard films on softer substrates corresponding to the case here, where H for MgO(001) is 9 ± 0.3 GPa.

The measured hardness values for our ScN films were found to be similar to those of TiN. Based on an intrinsic hardness for epitaxial TiN(001) of 20 ± 0.8 GPa,[15] we obtain $H=13.6\pm0.7$, 21.1 ± 1.1, and 24.4 ± 1.3 GPa for the 13, 20, and 50 eV ScN films, respectively. Thus, the highest-quality epitaxial ScN(002) layers grown in this study, deposited at 750 °C with $E_{N_2^+}=20$ eV and $J_{N_2^+}/J_{Sc}=14$, have hardnesses approximately 5% higher than TiN(001). The 111 textured polycrystalline layers grown with $E_{N_2^+}=13$ eV exhibit lower hardnesses due to their underdense columnar structure, as shown in Fig. 2. The porosity allows increased intra- and intercolumnar deformation under load. Similar tendencies have been reported for underdense TiN films.[36] In contrast, the 50 eV ScN films exhibit higher hardnesses due to their relatively high ion-irradiation-induced defect concentration which inhibits plastic flow.

Similarly, the elastic moduli of the ScN layers were determined using the measured Poisson ratio, $\nu_{ScN}=0.15$,[5] to be 302 ± 15, 356 ± 18, and 388 ± 20 GPa for 13, 20, and 50 eV films, respectively. Thus, the modulus of the highest quality ScN layer, $E_{N_2^+}=20$ eV, is 20% lower than that of TiN, 445 GPa.[15] This is reasonable based upon the 6.1% lattice constant difference between ScN and TiN ($a_{ScN}=0.4501$ nm and $a_{TiN}=0.4242$ nm) and the similarities in the bond structure. A more fundamental materials parameter than the elastic modulus E is the bulk modulus $K=E/3(1-2\nu)$, which from our data is 182 ± 40 GPa for ScN and, from data in Ref. 15, is 265 ± 23 GPa for TiN. These values are consistent with theoretical predictions, 146 and 257 GPa for ScN and TiN, respectively.[37] Based upon elementary force law considerations, K is expected to vary as r^{α}, where r is the interatomic spacing. Comparing TiN with our 20 eV epitaxial ScN layers, we obtain $\alpha=-6.4$. This is between the value predicted for purely ionic solids, $\alpha=-4$,[38] and that reported for dominantly covalent bonded TM carbides, $\alpha=-8.5$.[39] Our results therefore indicate that the bonding in ScN and TiN consists of a mixture of ionic and covalent components, in good agreement with predictions from band structure calculations showing that bond ionicity increases going from TM carbides to TM nitrides.[40] TiN also has an additional component of metallic bonding.

IV. CONCLUSIONS

ScN layers, 345 nm thick, were grown on MgO(001) substrates at 750 °C by ultrahigh vacuum magnetically unbalanced reactive magnetron sputter deposition in 5 mTorr pure N_2 discharges. The N_2^+ to Sc ratio incident at the substrate and growing film was maintained constant at 14, while the ion energy $E_{N_2^+}$ was varied from 13 to 50 eV. XRD, TEM, and XTEM analyses showed that film microstructure and texture were both very strongly dependent on $E_{N_2^+}$. During the early stages of growth, ScN films deposited with $E_{N_2^+}=13$ eV exhibited mixed 111 and 002 orientation. However, preferred orientation evolves rapidly toward a purely 111 texture within $\simeq 50$ nm as 002 grains grow out of existence. This occurs due to kinetic, rather than thermodynamic, effects and is associated with the longer residence time of Sc adatoms on low diffussivity 111 versus the higher diffusivity 002 planes. Increasing $E_{N_2^+}$ to 20 eV provides a sufficient increase in average adatom mobilities to overcome surface kinetic barriers and allows formation of purely 002-oriented films from the earliest stages. The $E_{N_2^+}=20$ eV films thus grow epitaxially on MgO with the relationship $(001)_{ScN}\|(001)_{MgO}$ and $[100]_{ScN}\|[100]_{MgO}$. Further increasing $E_{N_2^+}$ to 50 eV, however, results in films, which while still epitaxial, contain residual ion-irradiation-induced damage leading to large in-plane compressive strain and N_2-filled gas bubbles.

The relatively low growth temperatures, 750 °C, used in these experiments results in kinetic surface roughening during deposition. The surfaces are periodic with average sur-

face widths of ≃4 and 10 nm and corresponding in-plane correlation lengths of ≃30 and 50 nm for 20 and 50 eV layers, respectively. Nanopipes, which are first observed at film thicknesses of ≃5 nm and extend to the final surface, form due to atomic shadowing at cusps between adjoining growth mounds. Thus, the pipes have rectangular cross-sections along orthogonal ⟨100⟩ directions with widths of ≃1 nm and lengths of up to 15 and 25 nm for 20 and 50 eV films, respectively. The larger in-plane length scale for surface roughness of $E_{N_2^+}=50$ eV films results in a lower cusp density and therefore fewer nanopipes.

The hardness H and elastic modulus E of the 20 eV epitaxial ScN(001) layers, as determined from nanoindentation measurements, are 21.1 and 356 GPa, respectively. Combining the elastic modulus with the previously measured Poisson ratio for ScN[5] yields a bulk modulus K of 182 GPa. Increasing $E_{N_2^+}$ during film growth results in an increased film hardness due to the high residual defect concentration. Conversely, films grown with $E_{N_2^+}=13$ eV exhibit a lower apparent hardness due to their underdense structure allowing increased deformation under load.

ACKNOWLEDGMENTS

This work was supported by the U.S. Department of Energy, Division of Materials Science, under Grant No. DEFG02-ER9645439 through the University of Illinois Frederick Seitz Materials Research Laboratory and the Division of Materials Research, National Science Foundation. The authors also appreciate the use of the facilities of the MRL Center for Microscopy, which is partially supported by DOE, at the University of Illinois.

[1] D. Gall, I. Petrov, L. D. Madsen, J.-E. Sundgren, and J. E. Greene, J. Vac. Sci. Technol. A **16**, 2411 (1998).
[2] A. Neckel, P. Rastl, R. Eibler, P. Weinberger, and K. Schwarz, J. Phys. C **9**, 579 (1976).
[3] R. Eibler, M. Dorrer, and A. Neckel, Theor. Chim. Acta **63**, 133 (1983).
[4] L. I. Johansson, A. Callenas, P. M. Stefan, A. N. Christensen, and K. Schwarz, Phys. Rev. B **24**, 1883 (1981).
[5] D. Gall, I. Petrov, K. Järrendahl, and J. E. Greene (unpublished).
[6] J. E. Greene, J.-E. Sundgren, L. Hultman, I. Petrov, and D. B. Bergstrom, Appl. Phys. Lett. **67**, 2928 (1995).
[7] F. Adibi, I. Petrov, J. E. Greene, L. Hultman, and J.-E. Sundgren, J. Appl. Phys. **73**, 8580 (1993).
[8] N.-E. Lee, D. G. Cahill, and J. E. Greene, J. Appl. Phys. **80**, 2199 (1996).
[9] R. C. Powell, N.-E. Lee, Y.-W. Kim, and J. E. Greene, J. Appl. Phys. **73**, 189 (1993).
[10] I. Petrov, F. Adibi, J. E. Greene, W. D. Sproul, and W.-D. Münz, J. Vac. Sci. Technol. A **10**, 3283 (1992).
[11] A. V. Phelps, J. Phys. Chem. Ref. Data **20**, 557 (1991).
[12] B. Chapman, *Glow Discharge Processes* (Wiley, New York, 1980), p. 108.
[13] H. F. Winters, J. Chem. Phys. **43**, 926 (1965); **44**, 1472 (1966).
[14] R. L. Doolittle, Nucl. Instrum. Methods Phys. Res. B **15**, 344 (1985).
[15] H. Ljungcrantz, M. Odén, L. Hultman, J. E. Greene, and J.-E. Sundgren, J. Appl. Phys. **80**, 6725 (1996).
[16] W. C. Oliver and G. M. Pharr, J. Mater. Res. **7**, 1564 (1992).
[17] I. Petrov, A. Myers, J. E. Greene, and J. R. Abelson, J. Vac. Sci. Technol. A **12**, 2846 (1994).
[18] W. Lengauer, Solid State Chem. **76**, 412 (1988).
[19] The in-plane compressive strain was calculated using a weighted average of the measured 111 and 002 lattice constants along the film growth direction, the ScN Poisson ratio given in Ref. 5, and the elastic modulus of $E_{N_2^+}=13$ eV films determined from nanoindendation measurements discussed later in this article.
[20] B. Hajek, V. Brozek, and H. Duvigneaud, J. Less-Common Met. **33**, 385 (1973).
[21] H. Landolt and R. Börnstein, *Numerical Data and Functional Relationships in Science and Technlolgy, Group III* (Springer, Berlin, 1975), Vol. 7, Pt. B1, p. 27.
[22] J. O. Kim, J. D. Aschenbach, P. B. Mirkarimi, M. Shinn, and S. A. Barnett, J. Appl. Phys. **72**, 1805 (1992).
[23] L. Hultman, J.-E. Sundgren, and J. E. Greene, J. Appl. Phys. **66**, 536 (1989).
[24] H. Huang, G. H. Gilmer, and T. Díaz de la Rubia, J. Appl. Phys. **84**, 3636 (1998).
[25] Note that this discussion assumes that adatom mobilities are sufficient to sample multiple sites following deposition. In the limit of zero mobility, the arguments fail as film growth occurs in a ''hit and stick'' ballistic aggregation mode in which all orientations are equally probable and the resulting films are highly underdense due to severe atomic shadowing.
[26] G. Xue, H. Z. Xiao, M.-A. Hasan, J. E. Greene, and H. K. Birnbaum, J. Appl. Phys. **74**, 2512 (1993).
[27] N.-E. Lee, G. A. Tomasch, and J. E. Greene, Appl. Phys. Lett. **65**, 3236 (1994).
[28] N.-E. Lee, G. Xue, and J. E. Greene, J. Appl. Phys. **80**, 2199 (1996).
[29] D. J. Eaglesham, H.-J. Gossmann, and M. Cerullo, Phys. Rev. Lett. **65**, 1227 (1990).
[30] J. A. Stroscio, D. T. Piercee, M. D. Stiles, A. Zangwill, and L. M. Sander, Phys. Rev. Lett. **75**, 4246 (1995).
[31] B. W. Karr, I. Petrov, D. G. Cahill, and J. E. Greene, Appl. Phys. Lett. **70**, 1703 (1997).
[32] B. W. Karr, I. Petrov, P. Desjardins, D. G. Cahill, and J. E. Greene, Surf. Coat. Technol. **94/95**, 403 (1997).
[33] S. C. Wang and G. Ehrlich, Phys. Rev. Lett. **70**, 41 (1993) and **71**, 4177 (1993); G. Ehrlich, Surf. Sci. **331/333**, 865 (1995); A. Gölzhäuser and G. Ehrlich, Phys. Rev. Lett. **77**, 1334 (1996).
[34] E. P. Münger, V. Chirita, J. E. Greene, and J.-E. Sundgren, Surf. Sci. **355**, L325 (1996).
[35] L. Hultman, S. A. Barnett, J. E. Sundgren, and J. E. Greene, J. Cryst. Growth **92**, 639 (1988).
[36] D. S. Rickerby and P. J. Burnett, Thin Solid Films **157**, 195 (1988).
[37] W. A. Harrison and G. K. Straub, Phys. Rev. B **36**, 2695 (1987).
[38] N. W. Ashcroft and N. D. Mermin, *Solid State Physics* (Saunders College, Philadelphia, 1976), p. 413.
[39] L. E. Toth, *Transition Metal Carbides and Nitrides* (Academic, New York, 1971), p. 151.
[40] V. A. Gubanov, L. A. Ivanovsky, and V. P. Zhukov, *Electronic Structure of Refractory Carbides and Nitrides* (Cambridge University, Cambridge, 1994), p. 59.